Silicon (2018) 10:1443–1450
https://doi.org/10.1007/s12633-017-9624-z

ORIGINAL PAPER

A Double Core-shell Structure Silicon Carbon Composite Anode Material for a Lithium Ion Battery

Xiaoqiao Hu[1,2] · Shimin Huang[1] · Xianhua Hou[1,2] · Hedong Chen[1,2] · Haiqing Qin[3,4] · Qiang Ru[1,2] · Benli Chu[1,2]

Received: 18 April 2017 / Accepted: 21 August 2017 / Published online: 15 November 2017

Abstract Silicon with high theoretical specific capacity is a promising anode material, but the poor electronic conductivity and excessive volume expansion hinder its practical application. In order to solve this problem, a novel double core-shell structure composite Si/G/C-CVD coated by pitch pyrolysis and CVD (Chemical Vapor Deposition) carbon has been prepared. In the Si/G/C-CVD composite, nano-silicon particles and pitch particles are embedded on the surface of graphite particles, then the second carbon layer via CVD is added. The double carbon layer can protect nano-silicon particles from direct exposure to the electrolyte and enhance the electrochemistry performance during the lithium intercalation/extraction process. The as-prepared Si/G/C-CVD composite demonstrates superior electrochemical performance, with enhanced specific reversible capacity (688.44 mAh g^{-1} at 100 mA g^{-1}), excellent rate performance (261.66 mAh g^{-1} even at the specific current of 1.6A g^{-1}) and good cycle performance with little fading (91% after 155 cycles).

Keywords Double carbon layer · Electrochemical performances · Lithium ion battery · Silicon carbon composite

✉ Xianhua Hou
houxianhua@m.scnu.edu.cn

✉ Benli Chu
mountainchu@163.com

1 Guangdong Engineering Technology Research Center of Efficient Green Energy and Environment Protection Materials, South China Normal University, Guangzhou 510006, People's Republic of China

2 Guangdong Provincial Key Laboratory of Quantum Engineering and Quantum Materials, School of Physics and Telecommunication Engineering, South China Normal University, Guangzhou 510006, People's Republic of China

3 Guangxi Key Laboratory of Superhard Material, Guilin 541004, China

4 China Nonferrous Metal (Guilin) Geology And Mining Co., Ltd., Guilin 541004, China

1 Introduction

In recent years, much attention has been paid to energy storage devices. Among the many devices, electrochemical battery systems have offered a worthy solution. Lithium ion batteries show huge advantages of high energy density, long cycling lifetime and portability, and have been used in portable electronics and electric anode materials [1–5]. Nevertheless, beyond the current lithium ion battery technology, there is room for enhancing the battery performances by using alternative materials, modified electrolytes, as well as new strategies.

Among various anode materials, including Si, Sn, Ge and transitional oxides [6], Si has been considered as a promising anode material due to its highest theoretical capacity of 4200 mAh g^{-1}, relatively low delithiation potential and rich natural storage. However, the enormous volume change of Si during lithiation/delithiation can lead to Si particles cracking and electrode pulverization, furthermore bringing rapid capacity loss [7–10]. More seriously, during the initial cycle, the unstable SEI (solid electrolyte interphase) layer which reduces coulombic efficiency is formed [11–15].

To solve these problems, over the years, the researches on improving electronic conductivity of Si-based anode materials and buffering effects to avoid silicon expansion involve several aspects. Developing the nano-scale of Si is the most effective method [16–19]. In addition, there

are some pioneering works on Si–C composites with various carbonaceous materials, such as Si-amorphous carbon [20, 21], Si-carbon black [22, 23] and Si-carbon nanotubes (CNTs) [24, 25]. Core-shell structure of carbon-coated Si/C composite [26] and various Si-based composites combined with graphite [27–29] are good methods. For example, Vandenberg et al. [30] fabricated carbon-coated $LiCoO_2$ and $LiNiO_2$ compounds with a fast and very efficient microwave-assisted method. This method provided highly dispersed $LiCoO_2$ and $LiNiO_2$ within a highly contacted carbon material. A high specific charge of about 179 and 270 A h kg^{-1} was achieved for $LiCoO_2$ and $LiNiO_2$, respectively. Results show that the carbon-coated $LiCoO_2$ and $LiNiO_2$ display marked lower charge transfer resistance, higher lithium ion diffusion coefficient and much better rate capability than the original $LiCoO_2$ and $LiNiO_2$. The good electrochemical performance was attributed to the effects of carbon coating. Polypyrrole (PPy) provides an important conducting polymer. Recently, PPy has been employed in Si-based electrode materials in LIBs. For example, Liu et al. [31] fabricated a nanocomposite of molybdenum trioxide (alpha-MoO_3) nanobelts coated with a polypyrrole (PPy) in situ polymerization route. It was found that the PPy acted as a conducting matrix and a coating agent, which effectively improves the conductivity of the MoO_3 nanobelts and decreases the expansion of silicon.

As an alternative approach to overcome the drawbacks of Si, a Si/G/C-CVD composite with double carbon shell structure has been synthesized. The inner structure is of nano-silicon particles and pitch particles dispersed on the surface of artificial graphite. The double carbon structure provides two aspects. One is amorphous carbon coming from the coal-tar pitch on the surface of artificial graphite. The other is carbon coming from acetylene pyrolysis by the CVD method [32–34]. It was expected that the double carbon layer would restrain the volume expansion of nano-silicon particles. Moreover, the double carbon layer can enhance the electrical conductivity which makes the composite exhibit outstanding electrochemical performance during the lithiation/delithiation [35–37]. In addition, the process for the synthesis of the composite is green and beneficial to make a mass product for industry.

2 Experiment

2.1 Materials Preparation

2.1.1 Preparation of Nano-silicon Particles

The nano-silicon particles were obtained by Tekna's nanoparticle manufacturing device. The raw silicon particles are evaporated at high temperature and solidified rapidly in the quench zone. The size of nanoparticles is controlled by Tekna's unique quenching zone, and the diameter of nano-silicon particles is about 10-100 nm [33].

2.1.2 Preparation of Si/G Composite

As shown in Fig. 1, firstly, 0.4 g of nano-silicon particles was slowly added into 30 mL deionized water with magnetic stirring for 1 h at 50 °C. Secondly, 1.0 g of artificial graphite and 0.02 g of carboxymethylcellulose sodium (CMC) were dispersed in 40 mL deionized water with magnetic stirring for 1 h at 50 °C. Then, the above-mentioned two solutions were fully mixed to obtain solution A by the planetary mixer/deaerator (MAZERUSTAR KK-250S) which can mix the solution well by adjusting revolution speed and autorotation speed respectively (Fig. 1). The revolution role is to make the nano-silicon particles adequately dispersed on the artificial graphite, the effect of autorotation is to fully disperse the particles. The solution A was dried at 80 °C for 12 h. After that, the as-prepared precursor was calcined at 500 °C for 3 h and 900 °C for 3 h under N_2 atmosphere to receive the Si/G composite.

2.1.3 Preparation of Si/G/C-CVD Composite

Firstly, 0.14 g of pitch particles was added into 10 ml tetrahydrofuran (THF) and 0.011g of $Ni(CH_3COO)_2$ was added into 10 ml deionized water, and the two solutions mixed with magnetic stirring for 1 h at 50 °C, to obtain solution B. The solution B and solution A were mixed by adjusting revolution speed and autorotation speed of the planetary mixer/deaerator. The mixture was dried at 80 °C for 12 h before being calcined at 500 °C for 3 h and 900 °C for 3 h under N_2 atmosphere. The effect of this process is to carbonize the pitch into amorphous porous carbon, noted as Si/G/C composite. The precursors $Ni(CH_3COO)_2$ were reduced to NiO and Ni particles by H_2 at 700 °C, and then NiO and Ni acted as catalysts for the growth of the carbon layer by decomposition of ethylene in the following step. at an atmosphere of 1 h under Ar, then 20 min under C_2H_2/N_2 and finally 20 min under C_2H_2/Ar. As a result, the surface of the Si/G/C composite had a carbon layer, noted as the Si/G/C-CVD composite.

2.2 Materials Characterization

The X-ray diffraction (XRD) patterns of the Si/G/C-CVD were obtained with a Rigaku D/MAX-RC diffractometer. Scanning electron microscopy (SEM) (HITACHI S-4800) was used to analyze the morphology of the samples. Raman spectra was acquired using a WITEC Raman system with the wavelength of 100 to 1800 cm^{-1}. Thermogravimetric

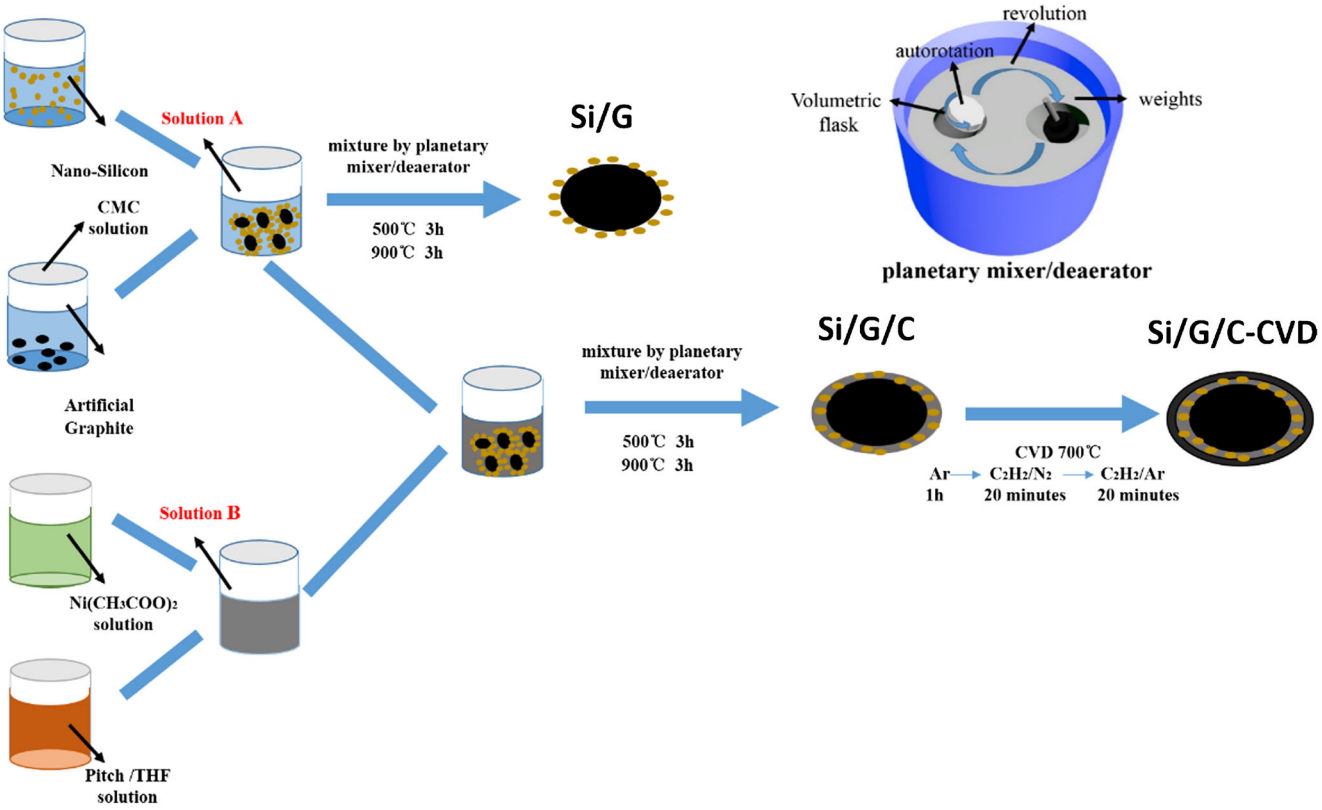

Fig. 1 Schematic diagram for the synthesis process of Si/G/C-CVD composite

(TG) analysis was used to test the content of Si in the samples from room temperature to 900 °C with a heating rate of 10 °C min^{-1} in air.

2.3 Electrochemical Measurements

For electrical characterizations, the electrode was assembled into CR2430 button cells in a glove box at the atmosphere of argon. The electrode consisted of active materials, binder (CMC) and conducting carbon (Super P) at a ratio of 8:1:1 by weight, and the solvent is distilled water. The electrolyte solution was 1 mol L^{-1} of $LiPF_6$ which was dispersed in a mixed solvent of diethyl carbonate (DC), ethylene carbonate (EC), and ethylmethyl carbonate (EMC) at a volume ratio of 1:1:1. The galvanostatic charging/discharging property of the assembled cell was evaluated by an automatic battery testing system (LANDCT2001A) with a voltage of 0.01 V to 2.5 V at a current density of 100 mA g^{-1}. The electrochemical workstation (Solartron 1470E electrochemistry system) was used to record cyclic voltammetry (CV) data at the scan rate of 0.1 mV s^{-1}. Electrochemical impedance spectra (EIS) tests were recorded by a CHI604D Electrochemistry System with the frequency range of 100 KHz to 10 MHz using an electric IM6ex impedance analyzer.

3 Results and Discussion

3.1 Phase Composition

As shown in Fig. 2a, the structural characteristic of Si/G/C-CVD composite was analyzed using X-ray diffraction. All reflections are shown in the Bragg peaks of graphite (2θ = 26.4°, 42.2°, 44.4°, 50.5°, 54.5°, 59.7°, 77.2°, 83.2° and 86.8°) and crystalline Si (2θ = 28.4°, 47.3°, 56.1°, 69.1°, 76.4° and 88.0°), which corresponds to the lattice planes of (002), (100), (101), (102), (004), (103), (110), (112), (006) and (111), (220), (311), (400), (331), (422) [38, 39]. The results demonstrate that there are no peaks corresponding to SiC (compound which consists of Si and carbon), proving that the synthesis process did not produce chemical reaction. In addition, no obvious peaks Ni can be observed because the content of Ni is very low in the composite.

The Raman spectra of Si/G/C-CVD composite is shown in Fig. 2b, which illustrates the degree of graphitization of carbon. Around 1300-1600 cm^{-1}, there are two typical large peaks. One peak is at 1340 cm^{-1}, indicating the amorphous structure of carbon of the D band; the other peak is at 1585 cm^{-1}, corresponding to the graphite structure of carbon of the G band which demonstrates the ordered arrangement of the carbon lattice. The intensity of the G band to the D band

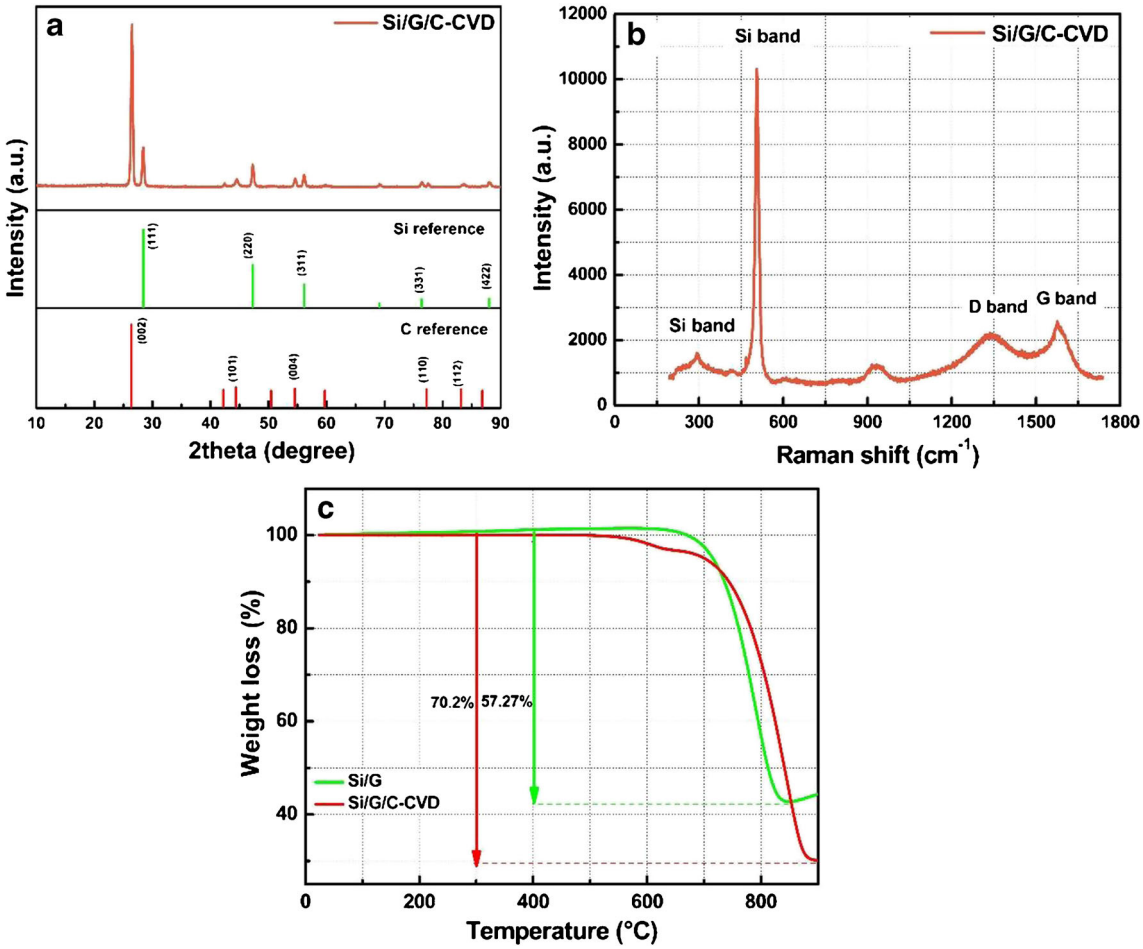

Fig. 2 **a** XRD pattern of Si/G/C-CVD composite. **b** Raman spectra of Si/G/C-CVD composite. **c** TGA curve of Si/G/C-CVD composite and Si/G composite

(I_G/I_D) is 1.18. The result displays a high degree of graphitization of the carbon. In addition, one sharp peak at 505 cm^{-1} and the other gentle peak at 295 cm^{-1}, correspond to the silicon phase.

Thermogravimetric (TG) analysis was used to roughly determine the content of Si in the Si/G/C-CVD composite and the Si/G composite between room temperature and 900 °C in air. The Si/G/C-CVD composite and Si/G composite show a sharp drop after 640 °C due to the oxidation of carbon materials, and eventually lose about 70.2% and 57.27% respectively, which is in agreement with the designed results.

3.2 Morphology Analysis

The morphology features of nano-silicon particles, artificial graphite particles and Si/G/C-CVD composite were examined by SEM shown in Fig. 3a–d. Figure 3a shows the nano-silicon particles with the range of 20 to 100 nm. Artificial graphite particles with the size of 10 to 18 μm are displayed in Fig. 3b. Figure 3c and d show the SEM images of the Si/G/C-CVD composite. In Fig. 3d, there are artificial graphite particles and nano-silicon particles, and the surface of the artificial graphite particles is rough, the reason is that nano-silicon particles are equably adhered on the surface, which is forming the core-shell structure.

3.3 Electrochemical Performance

As shown in Fig. 4a, the charging/discharging curve of the Si/G/C-CVD electrode demonstrates super performance. During the first cycling, the charging/discharging capacities are 543.88 mAh g^{-1}/688.44 mAh g^{-1}. The initial coulombic efficiency is 79%, which is ascribed to the formation of a SEI film. The initial discharging curve has two broad plateaus, which are at 0.1 V and 0.4 V respectively, corresponding to the formation of lithium silicon alloy. For the 2nd cycle, the charging/discharging capacities are 529.45 mAh g^{-1}/563.495 mAh g^{-1} with the coulombic efficiency of 94%. And for the 50th, the charging/discharging capacities are 634.58 mAh g^{-1}/646.37 mAh g^{-1} and the coulombic efficiency is 98%. As a result, the Si/G/C-CVD

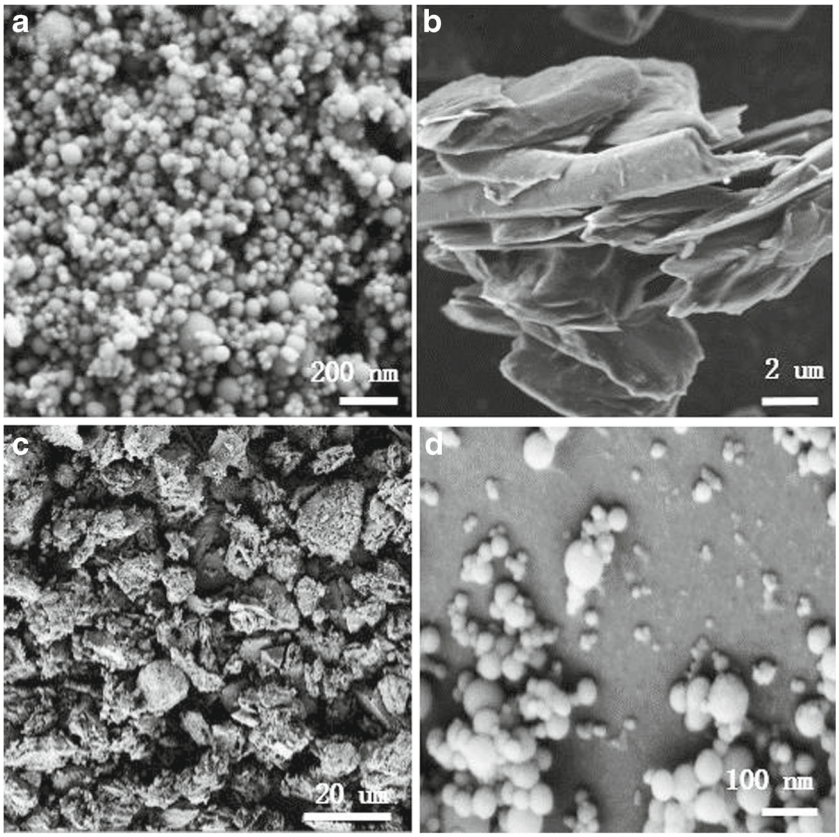

Fig. 3 SEM image of (**a**) nano-silicon particles. SEM image of (**b**) artificial graphite particles. SEM images of (**c**) and (**d**) Si/G/C-CVD composite

electrode shows good capacity retention and the capacity is increased during the cycling process [46, 47]. The reason is that the Si/G/C-CVD electrode has a stable double carbon layer structure to buffer the volume expansion.

As shown in Fig. 4b, the cycling stabilities of nano-silicon, Si/G and Si/G/C-CVD electrodes were tested during the discharge/charge processes at the current density of 100 mA g^{-1} between 0.01 and 1.5 V. At the first cycle, the nano-silicon electrode gave a much higher discharging capacity of 3424.94 mAh g^{-1} than that of the Si/G electrode and Si/G/C-CVD electrode. But after only 43 cycles, the nano-silicon electrode dropped to 28.63 mAh g^{-1}, showing 1.35% capacity retention. The reason is that as the cycling increased, the nano-silicon electrode shows excessive volume expansion, and the crystal structure of nano-silicon is broken. In contrast, the initial discharging capacity of the Si/G electrode and Si/G/C-CVD electrode are 688.44 mAh g^{-1} and 762.55 mAh g^{-1}, and after 155 cycles, the retentions are 61.01% and 91% respectively. It is important that as the cycles increase, the Si/G/C-CVD electrode shows good cyclic stability. Instead, the capacity of the Si/G electrode decreases [38, 39, 42, 43].

As shown in Fig. 4c, in order to have a stronger contrast of the Si/G electrode and Si/G/C-CVD electrode, the rate performances of the Si/G electrode and Si/G/C-CVD electrode were tested in a half cell. For the first 10 cycles, at the current density of 100 mA g^{-1}, the capacity of the Si/G electrode (658.04 mAh g^{-1}) is higher than that of the Si/G/C-CVD electrode (641.26 mAh g^{-1}). This is because the Si/G/C-CVD electrode has a stable structure of double carbon layer. As the current density increased, the Si/G/C-CVD electrode shows prominent rate capacity stability. At the current density of 200 mA g^{-1}, 400 mA g^{-1}, 800 mA g^{-1} and 1.6 A g^{-1}, the discharging capacities of the Si/G/C-CVD electrode are 509.30 mAh g^{-1}, 458.48 mAh g^{-1}, 343.7 mAh g^{-1} and 261.76 mAh g^{-1} respectively. In contrast the discharging capacities of the Si/G electrode are 426.9 mAh g^{-1}, 293.97 mAh g^{-1}, 183.40 mAh g^{-1}, and 69.57 mAh g^{-1} respectively at the same current density gradient. Once the current density recovers 100 mA g^{-1}, the Si/G/C-CVD electrode shows high reversible discharging capacity of 551.68 mAh g^{-1}. Instead, the Si/G electrode exhibits a low reversible discharging capacity of 548.2 mAh g^{-1}. Moreover, as the cycles increased, the discharging capacity of the Si/G electrode gradually fades. On the contrary, the Si/G/C-CVD electrode rises with a very short span and after 82 cycles the capacity is stable, owing to the protection of the double carbon layer.

Cyclic voltammetry (CV) curves of the Si/G/C-CVD electrode are shown in Fig. 4d. As shown in the first cycle, there are two broad reduction peaks during 0.25V to 1.8V. Especially, at 0.63 V and 1.62 V the two sharp reduction

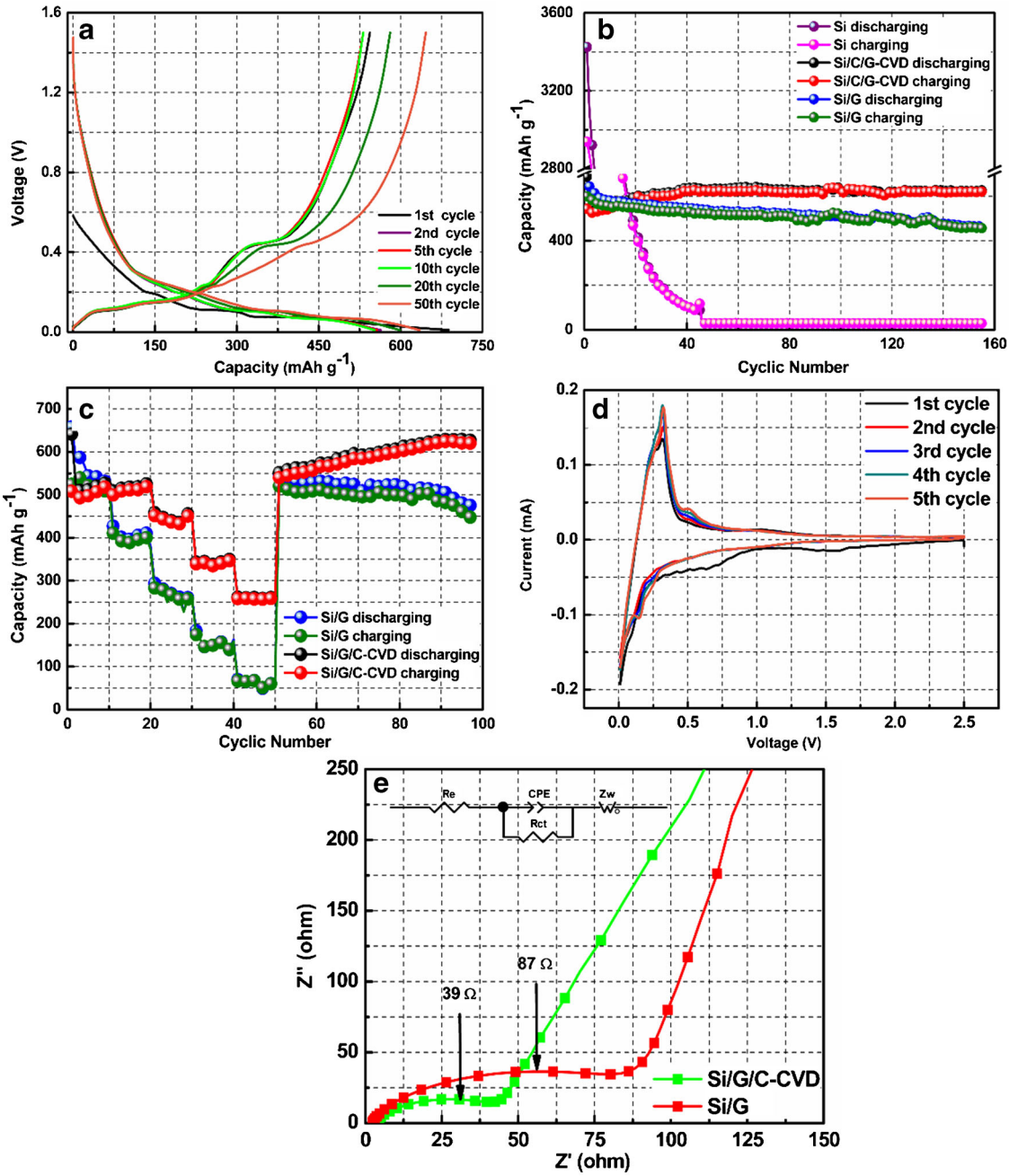

Fig. 4 Charging/discharging curve of (**a**) Si/G/C-CVD electrode. Cycling profiles of (**b**) Si/G/C-CVD electrode, Si/G electrode and nano-silicon particles electrode at 100 mA g^{-1}. Rate capabilities at various rates for (**c**) the Si/G electrode and Si/G/C-CVD electrode. CV curves of (**d**) Si/G/C-CVD electrode. Impedance spectra of (**e**) Si/G electrode and Si/G/C-CVD electrode

peaks are obvious. That is caused by the formation of a SEI film which is an insulator for electrons and an excellent conductor for lithium ions. In addition, the two reactions of alloying and de-alloying Li_xSi can react freely. However, the formation of the SEI film also consumes lithium ions and leads to the fading of specific capacity. For the subsequent cycles, the two broad reduction peaks disappear and the CV curves are almost similar [11–15, 44, 45]. It proves that the SEI film during the processes of alloying and de-alloying Li_xSi is stable. At the anodic scans, there are two anodic peaks which are at 0.37 V and 0.49 V. The phenomenon corresponds to the extraction of lithium ions from the anode. At 0.17 V, there is a sharp cathodic peak, responding to the formation of Li_xSi during the de-insert lithium ions reaction.

As shown in Fig. 4e, in order to show the better electrochemical properties the Si/G/C-CVD electrode, Si/G/C-CVD electrode and Si/G electrode were examined by an electrochemical impedance spectrum (EIS) method in open

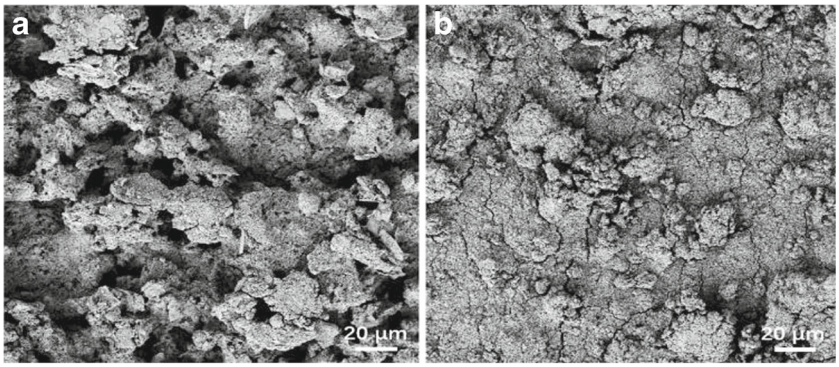

Fig. 5 SEM image of Si/G/C-CVD composite anode uncycled and after 150 cycles

circuit potential. The Nyquist plots consist of three parts. The intercept on the Z real axis in the high frequency region is attributed to the solid electrolyte interphase (SEI) film resistance, ohmic resistance and film contact resistance (Rs); while the semicircle in the medium frequency region is attributed to the charge transfer impedance on the electrode/electrolyte interface (Rct); and the slope line of the low frequency region corresponds to the Warburg impedance (Wo), which is ascribed to the solid-state diffusion of lithium ions in the electrode materials [39–41]. It is clear that the charge transfer resistance of the Si/G electrode is much larger than that of the Si/G/C-CVD electrode. A good electronic contact between nano-silicon particles and amorphous carbon was obtained during the carbonization process, and the charge transfer resistance is improved.

To have a more detailed explanation of the superiority of the as-prepared composite, the morphological changes of the Si/G/C-CVD electrode were examined by SEM. Figure 5a and b are the uncycled electrode and the electrode after 150 cycles respectively. Figure 5a shows a rough surface. But after 150 cycles, the surface is relatively smooth in Fig. 5b. This is because of the formation of the SEI film on the surface of the Si/G/C-CVD electrode. As seen from Fig. 5b, the structure of the Si/G/C-CVD composite is maintained well, demonstrating the enhanced cycling stability [48, 49].

4 Conclusions

In summary, a Si/G/C-CVD composite was successfully designed via the CVD method and applied in LIBs as an anode, showing good cycling stability and excellent rate performance. This result is attributed to the special structure of the double carbon layer which is providing electronic conductivity and offering extra volume for the expansion of nano-silicon particles. In addition, the structure of nano-silicon particles embedded into the surface of artificial graphite is also efficiently accommodating the large volume expansion of nano-silicon particles during the charge/discharge process. Therefore, the Si/G/C-CVD composite is expected to be a potential anode material to replace current graphite in lithium ion batteries.

Acknowledgments This work is supported by the union project of the National Natural Science Foundation of China and Guangdong Province (No. U1601214), the Scientific and Technological Plan of Guangdong Province (2016A050503040, 2016B010114002 2017B090901027), and the Scientific and Technological Plan of Guangzhou City (201607010322).

References

1. Deshpande R, Cheng YT, Verbrugge MW (2010) Modeling diffusion-induced stress in nanowire electrode structures. J Power Sources 195:5081–5088
2. Wang JY, Hou XH, Zhang M, Li YN, Wu YP, Liu X et al (2017) 3-Aminopropyltriethoxysilane-Assisted Si@SiO2/CNTs hybrid microspheres as superior anode materials for li-ion batteries. Silicon 9:97–1043
3. Jeong G, Kim YU, Kim H, Kim YJ, Sohn HJ (2011) Prospective materials and applications for Li secondary batteries. Energy Environ Sci 4:1986–2002
4. Armand M, Tarascon JM (2008) Building better batteries. Nature 451:652–657
5. Dunn H, Kamath JM (2011) Electrical energy storage for the grid: a battery of choices. Science 334:928–935
6. Wu H, Cui Y (2012) Designing nanostructured Si anodes for high energy lithium ion batteries. Nano Today 7:414–429
7. Das B, Reddy MV, Chowdari BVR (2016) SnO and SnO@CoO nanocomposite as high capacity anode materials for lithium ion batteries. Mater Res Bull 74:291–298
8. Zhou Y, Jiang X, Chen L, Yue J, Xu H, Yang J et al (2014) Novel mesoporous silicon nanorod as an anode material for lithium ion batteries. Electrochim Acta 127:252–258
9. Zhang CJ, Gu L, Kaskhedikar N, Cui GL, Maier J (2013) Preparation of Silicon@Silicon Oxide core-shell nanowires from a silica precursor toward a high energy density Li-Ion battery anode. ACS Appl 5:12340–12345
10. Wang X, Wen Z, Liu Y, Xu X (2009) Preparation and characterization of a new nanosized silicon–nickel–graphite composite as anode material for lithium ion batteries. J Power Sources 189:121–126
11. McDowell MT, Ryu I, Lee SW, Wang WC, Nix WD, Cui Y (2012) Studying the kinetics of crystalline silicon nanoparticle lithiation with in situ transmission electron microscopy. Adv Mater 24:6034–6041

12. Lee BS, Yang HS, Jung H, Jeon SY, Jung C, Kim SW et al (2014) Novel multilayered 1-D nanostructure exhibiting the theoretical capacity of silicon for a super-enhanced lithium-ion battery. Nanoscale 6:5989–5998
13. Zhang H, Qin X, Wu J, He YB, Du H, Li B et al (2015) Electrospun core-shell silicon/carbon fibers with internal honeycomb-like conductive carbon framework as anode for lithium ion batteries. J Mater Chem 3:7112–7120
14. Reddy MV, Wen BLW, Loh KP, Chowdari BVR (2013) Energy storage studies on InVO4 as high performance anode material for Li-Ion batteries. ACS Appl Mater 5:7777–7785
15. Das B, Reddy MV, Chowdari BVR (2013) Li-storage of Fe3O4/C composite prepared by one-step carbothermal reduction method. J Alloy Compd 565:90–96
16. Zhong H, Zhan H, Zhou YH (2014) Synthesis of nanosized mesoporous silicon by magnesium-thermal method used as anode material for lithium ion battery. J Power Sources 262:10–14
17. Liang J, Li X, Zhu Y, Guo C, Qian Y (2015) Hydrothermal synthesis of nano-siliconrom a silica sol and its use in lithium ion batteries. Nano Res 8:1497–1504
18. Liu N, Lu Z, Zhao J, McDowell MT, Lee HW, Zhao W et al (2014) A pomegranate-inspired nanoscale design for large-volume-change lithium battery anodes. Nat Nanotechnol 9:187–192
19. Zhong H, Zhan H, Zhou YH (2014) Synthesis of nanosized mesoporous silicon by magnesium-thermal method used as anode material for lithium ion battery. J Power Sources 262:10–14
20. Xu ZL, Zhang B, Kim JK (2014) Electrospun carbon nanofiber anodes containing monodispersed Si nanoparticles and graphene oxide with exceptional high rate capacities. Nano Energy 6:27–35
21. Yun QB, Qin XY, Lv W, He YB, Li BH, Kang FY et al (2015) "Concrete" inspired construction of a silicon/carbon hybrid electrode for high performance lithium ion battery. Carbon 93:59–67
22. Magasinski A, Dixon P, Hertzberg B, Kvit A, Ayala J, Yushin G (2010) High-performance lithium-ion anodes using a hierarchical bottom-up approach. Nat Mater 9:353–358
23. Chen Y, Nie M, Lucht BL, Saha A, Guduru PR, Bose A et al (2013) Stable silicon/carbon anodes for lithium-ion batteries prepared using emulsion-templated directed assembly. ACS Appl Mater Interfaces 6:4678–4683
24. Yu WJ, Liu C, Hou PX, Zhang L, Shan XY, Li F et al (2015) Lithiation of silicon nanoparticles confined in carbon nanotubes. ACS Nano 9:5063–5071
25. Li Y, Xu GJ, Xue GL, Zhang S, Yao YF, Lu Y (2015) Enhanced rate capability by employing carbon nanotube-loaded electrospun Si/C composite nanofibers as binder-free anodes. J Electrochem Soc 160:A528–A534
26. Zhang T, Fu LJ, Gao J, Wu VP, Wu HQ et al (2005) Preparation and characterization of carbon coated silicon nanoparticle as anode material for Li-ion batteries. Nat Sci 9:903–907
27. Fu Y, Manthiram A (2013) Silicon nanoparticles supported on graphitic carbon paper as a hybrid anode for Li-ion batteries. Nano Energy 2:1107–1112
28. Ng SH, Wang J, Wexler D, Chew SY, Liu HK (2007) Amorphous carbon-coated silicon nanocomposites: a low-temperature synthesis via spray pyrolysis and their application as high-capacity anodes for lithium-ion batteries. J Phys Chem C 11131–11138
29. Xie J, Wang G, Huo Y, Zhang S, Cao G, Zhao X (2014) Nanostructured silicon spheres prepared by a controllable magnesiothermic reduction as anode for lithium ion batteries. Electrochim Acta 135:94–100
30. Vandenberg A, Hintennach A (2015) Comparative microwave-assisted synthesis of carbon-coated $LiCoO_2$ and $LiNiO_2$ for lithium-ion batteries. Russ J Electrochem 4:310–317
31. Liu Y, Zhang BH, Yang YQ, Chang Z, Wen ZB, Wu YP (2013) Polypyrrole-coated alpha-MoO_3 nanobelts with good electrochemical performance as anode materials for aqueous super capacitors. J Mater Chem A43:13582–13587
32. Ge MY, Rong JP, Fang X, Zhou CW (2012) Porous doped silicon nanowires for lithium ion battery anode with long cycle life. Nano Lett 12:2318–2323
33. Sim S, Oh P, Park S, Cho J (2013) Critical thickness of SiO2 coating layer on Core@Shell Bulk@Nanowire Si anode materials for Li-Ion batteries. Adv Mater 25:4498–4503
34. Bang BM, Lee JI, Kim H, Cho J, Park S (2012) High-performance macroporous bulksilicon anodes synthesized by template-free chemical etching. Adv Energy Mater 2:878–883
35. Huang ZX, Wang Y, Wong JI, Shi WH, Yang HY (2015) Synthesis of self-assembled cobalt sulphide coated carbon nanotube and its superior electrochemical performance as anodes for Li-ion batteries. Electrochim Acta 167:388–395
36. Shao L, Shu J, Wu K, Lin X, Li P, Shui M et al (2014) Low pressure preparation of spherical Si@C@CNT@C anode material for lithium-ion batteries. J Electroanal Chem 727:8–12
37. Chen HD, Hou XH, Qu LN, Qin HQ, Ru Q, Huang Y et al (2016) Electrochemical properties of core–shell nano-Si@carbon composites as superior anode materials for high-performance Li-ion batteries. J Mater Sci 16:5518–5527
38. Lai J, Guo H, Wang Z, Li X, Zhang X, Wu F (2012) Preparation and characterization of flake graphite/silicon/carbon spherical composite as anode materials for lithium-ion batteries. J Alloys Compd 530:30–35
39. Zhou Y, Tian Z, Fan R, Zhao S, Zhou R, Guo H, Wang Z (2015) Scalable synthesis of Si/SiO2@C composite from micro-silica particles for high performance lithium battery anodes. Powder Technol 284:365–370
40. Wang G, Liu YZ, Liu P (2011) Co2SnO4-multiwalled carbon nanotubes composites as highly reversible anode material for lithium-ion batteries. Ectrochim Acta 56:9515–9529
41. Macdonald DD (2006) Reflections on the history of electrochemical impedance spectrum. Electrochim Acta 51:1376–1385
42. Fang G, Kaneko S, Liu W, Xia B, Sun H, Zhang R et al (2013) Facile synthesis of nitrogen-doped carbon coated CoSnO3 via hydrothermal carbonization of carboxylated chitosan as anode materials for lithium-ion batteries. Appl Surf Sci 283:963–967
43. Zhang J, Liang J, Zhu Y, Wei D, Fan L, Qian Y (2014) Arrays of sealed silicon nanotubes as anodes for lithium ion batteries. J Mater Chem A2:2728–2734
44. Xu Y, Zhu Y, Han F, Luo C, Wang C (2015) 3D Si/C fiber paper electrode fabricated using a combined electrospray/electrospinning technique for Li-ion batteries. Adv Energy Mater 5:753–765
45. Li M, Gu J, Feng X, He H, Zeng C (2015) Amorphous-silicon@silicon oxide/chromium/carbon as an anode for lithium-ion batteries with excellent cyclic stability. Electrochim Acta 164:163–170
46. Su M, Wang Z, Guo H, Li X, Huang S, Gan L (2013) Silicon flake graphite and phenolic resin-pyrolyzed carbon based Si/C composites as anode material for lithium-ion batteries. Adv Powder Technol 24:921–925
47. Huang ZX, Wang Y, Wong JI, Shi WH, Yang HY (2015) Synthesis of self-assembled cobalt sulphide coated carbon nanotube and its superior electrochemical performance as anodes for Li-ion batteries. Electrochim Acta 167:388–395
48. Zhang H, Qin X, Wu J, He YB, Du H, Li B et al (2015) Electrospun core-shell silicon/carbon fibers with internal honeycomb-like conductive carbon framework as anode for lithium ion batteries. J Mater Chem 3:7112–7120
49. Wen W, Lin H, Chen X, Ren J, Zhang Z, Qiu L et al (2014) Flexible and stable lithium ion batteries based on three-dimensional aligned carbon nanotube/silicon hybrid electrodes. J Mater Chem A 2:93